Breakdown of Landau-Ginzburg-Wilson Scheme for Phase Transitions Between Orbital-Current Phases and Zero-gap Semiconductors

Moyuru Kurita, Youhei Yamaji, and Masatoshi Imada
Department of Applied Physics, University of Tokyo, Hongo, Bunkyo-ku, Tokyo, 113-8656, Japan. and
CREST, JST, Hongo, Bunkyo-ku, Tokyo, 113-8656, Japan.
(Dated: January 6, 2012)

We show that Landau-Ginzburg-Wilson (LGW) scheme for symmetry-breaking transitions breaks down when spontaneous orbital currents cause quantum phase transitions from zero-gap semiconductors such as Dirac fermions to topological insulator (TI) or Chern insulator (CI). *Topology change* generates unconventional universality characterized by mean-field critical exponents $\beta = n/(d-n)$ and $\delta = d/n$ arising from free-energy singularity $|\zeta|^{d/n+1}$ that induces enhanced quantum fluctuations. Here, ζ, d, and n are intensity of the orbital current, spatial dimension, and band-dispersion exponent, respectively.

PACS numbers: 05.30.Rt,71.10.Fd,73.43.Lp,71.27.+a

Introduction. — Critical phenomena of phase transitions are classified into a small number of universality classes. For such symmetry-breaking transitions, the LGW scheme is extremely successful [1, 2]. Usual Fermi sea of electrons in crystalline solids, a *vacuum* for particle-hole excitations, is known to be unstable in the presence of electron-electron interactions, leading to spontaneous symmetry breakings. Competitions of different spontaneous symmetry breakings, for instance, magnetism and superconductivity are the subject of extensive studies on strongly correlated electron systems. Although it has a rich diversity, most phase transitions accompanying the spontaneous symmetry breakings are primarily described by the LGW framework [1, 2]. In spite of its great success, however, the LGW scheme has recently been challenged from various viewpoints, especially in strongly correlated electrons [3–5].

Contrary to the conventional Fermi sea, particle-hole excitations sometimes behave as massless Dirac fermions as realized in graphene [6] and at surfaces of TI [7–10]. These *zero-gap semiconductors* attract much attention because of peculiar transport properties, such as ballistic transport [11] and quantum Hall effects [12, 13]. Unlike the usual Fermi sea, band crossing points (Fermi points of the zero-gap semiconductors) are protected by certain symmetries [7, 14] and thus are inferred to have weaker instabilities [11, 15].

However, the zero-gap semiconductors are sensitive to the spin-orbit interaction, and time-reversal-symmetry broken fields such as magnetic flux. These stabilize topologically nontrivial phases as TI for the former and quantum Hall insulators (or CI) [12] for the latter. It induces microscopic loop of spin (or charge) currents, for which we inclusively call *orbital currents*. We call phase transitions between the orbital-current phases (TI or CI) and zero-gap semiconductors orbital-current transition (OCT).

Even without such external triggers, electron-electron interactions are proposed to cause spontaneous symmetry breakings generating the orbital currents [16–19]. This spontaneous-orbital-current phase is called a topological Mott insulators (TMI). We call transitions to TMI, topological Mott transitions(TMT).

In this Letter we propose that the universality class of OCT including TMT is unprecedented, because of the involvement of the topological change beyond the concept of the symmetry breaking, which causes non-LGW type singularities. This opens new avenues of studies on quantum critical phenomena and provides a clue for potential applications of TI (or CI) and its transitions.

Differently from the Dirac fermions, quadratic band-crossing points have also been recently discussed [17, 18, 20, 21]. In general, zero-gap semiconductors may be described by a simple dispersion ϵ_+ and ϵ_- as functions of momenta k, $\epsilon_\pm = \pm v_\pm k^n$, ($n = 1$ for Dirac fermions and $n = 2$ for quadratic band crossings) with a double degeneracy at $k = 0$. We present a comprehensive theory with dependences on n and spatial dimensionality d.

In fact, Dirac fermions appear in honeycomb [12] and diamond lattices [19], while quadratic band-crossing points show up in kagomé [17, 20], and pyrochlore lattices [18, 21](Fig.1(a)-(c)), where, only in the pyrochlore lattice, three bands touch each other instead of two.

The orbital currents make the band-crossing point massive (Fig.1(d)) in the simplest case as,

$$\epsilon_\pm = \pm v_\pm k^n \to \pm\sqrt{m^2 + v_\pm^2 k^{2n}}. \tag{1}$$

A mass m is scaled by, as we will discuss later, the orbital current ζ multiplied by intersite Coulomb repulsion V; $m \propto V\zeta$. Orbital currents are sketched in Fig.1(e)-(g) (see also S.1 of Supplemental Material for details [22]).

Model and Method. —To understand the criticality of OCT, especially at $T = 0$, we expand the free energy F in terms of the order parameter ζ based on a microscopic hamiltonian and realistic band dispersions. Although we formally follow the spirit of LGW expansion, we will see

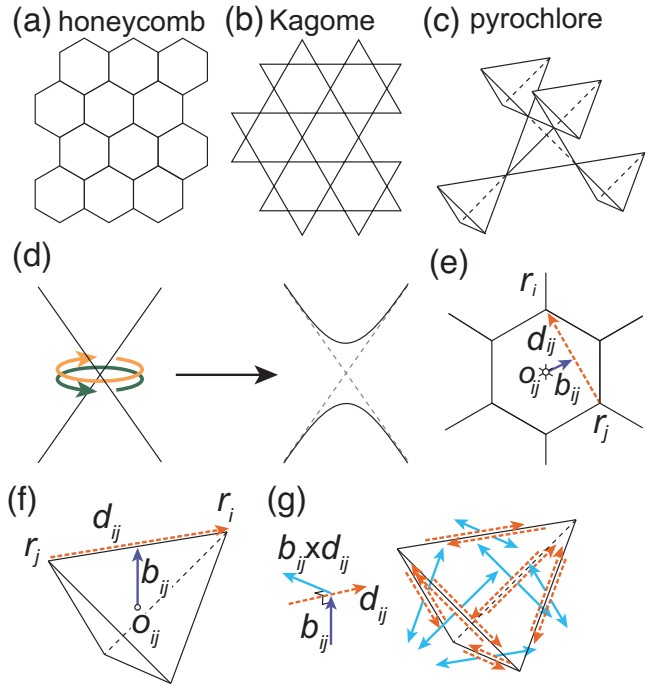

FIG. 1. (color online) (a) Honeycomb, (b) kagomé and (c) pyrochlore lattice structures. (d) Schematics showing how degeneracy at a band-crossing point is lifted. The origin of the gap formation is understood from the lifting of the degeneracy related to the lattice symmetry. For example, in 2D lattices like the honeycomb and kagomé lattices, the clock- and counterclock-wise rotating electrons are doubly degenerate at the band-crossing point. The orbital currents break the symmetry, and lift the 2-fold degeneracy between them, leading to a gap. The loop current in this momentum space is equivalent to that in the real space shown in (g). Spin-orbital-current configurations on a hexagon (e) and a tetrahedron (f): Along each nearest neighbor bond (r_i, r_j), opposite spins on the directions $\pm\vec{b}_{ij} \times \vec{d}_{ij}$ flow in the opposite directions (g). Here, we define $\vec{d}_{ij} = \vec{r}_i - \vec{r}_j$ and $\vec{b}_{ij} = (\vec{r}_i + \vec{r}_j)/2 - \vec{o}_{ij}$ with $\vec{o}_{ij}$ being the gravity center of the hexagon (e) (tetrahedron (f)). In (g), all the vectors schematically illustrate only the correct directions while the lengths are not correct.

later that F has a singularity expressed by $|\zeta|^{d/n+1}$ that disrupts the LGW scheme.

As a microscopic hamiltonian, we study an extended Hubbard model,

$$\hat{H} = -t \sum_{\langle i,j\rangle\sigma} \hat{c}^\dagger_{i\sigma}\hat{c}_{j\sigma} + U\sum_i \hat{n}_{i\uparrow}\hat{n}_{i\downarrow} + \sum_{i,j}\frac{V_{ij}}{2}\hat{n}_i\hat{n}_j, \quad (2)$$

where $\hat{c}^\dagger_{i\sigma}$ ($\hat{c}_{i\sigma}$) is a creation (annihilation) operator for a σ-spin electron, $\hat{n}_i = \hat{n}_{i\uparrow} + \hat{n}_{i\downarrow}$ is an electron density operator, $\langle i,j\rangle$ is a pair of nearest-neighbor sites, and U (V_{ij}) are an on-site (off-site) Coulomb repulsion. We only consider the nearest ($V_{ij} = V_1$) and 2nd ($V_{ij} = V_2$) neighbor interactions for V_{ij}, for simplicity.

The Hartree-Fock decoupling of the interaction (V) term in Eq.(2) is naturally described by a product of two spontaneous orbital currents that preserve lattice symmetries[16, 18]. Among possible mean fields, two types of loop orbital currents exist: One is a mean field of the spin-orbital current,

$$\zeta_s = \frac{i}{2}\sum_{\alpha,\beta}\left\langle \hat{c}^\dagger_{j\beta}\hat{c}_{i\alpha}\right\rangle \frac{\vec{b}_{ij}\times\vec{d}_{ij}}{|\vec{b}_{ij}\times\vec{d}_{ij}|}\cdot\vec{\sigma}_{\alpha\beta}, \quad (3)$$

which creates time-reversal-symmetric topological insulators and the other is a mean field of the charge-orbital current,

$$\zeta_c = \frac{i}{2}\sum_{\sigma}\left\langle \hat{c}^\dagger_{j\sigma}\hat{c}_{i\sigma}\right\rangle \left[\frac{\vec{b}_{ij}\times\vec{d}_{ij}}{|\vec{b}_{ij}\times\vec{d}_{ij}|}\right]_z, \quad (4)$$

which induces time-reversal-symmetry broken Chern insulators. For definitions of $\vec{b}_{ij}$ and $\vec{d}_{ij}$, see Fig.1(g) (see also S.1 of Supplemental Material [22]). We note that the form (3) is identical to the spin-orbit interaction uniquely allowed by the lattice symmetry and the time-reversal invariance [22].

Now in the Hartree-Fock theory, other types of orders such as the antiferromagnetic and charge-density-wave orders compete. In the plane of U, V and t, phase diagrams clarified on various lattices after considering the competition indeed contain the region of stable symmetry breaking into either $\zeta_s \neq 0$ or $\zeta_c \neq 0$ phases within realistic parameters [16, 18].

Results. — The resultant free energy, $f[\zeta]$ is expanded by ζ (for both $\zeta = \zeta_c$ and $\zeta = \zeta_s$) as

$$f[\zeta] - f[0] = -\lambda\zeta + a\zeta^2 + b_\pm f_s[\zeta] + (\text{higher order}), \quad (5)$$

for small ζ close to OCT. Here a and $b_\pm$ are constants. We add a spin-orbit coupling or magnetic flux λ conjugate to ζ, as a straightforward analogue of magnetic fields in magnetic phase transitions. In addition to the regular term proportional to a, the singular part $f_s[\zeta] \propto |\zeta|^{d/n+1}$ emerges with logarithmic corrections. For details of expansion and derivation see Table I and S.2 of Supplemental Material [22]. The coefficient b_+ for $\zeta > 0$ is not necessarily equal to b_- for $\zeta < 0$. The expansion (5) is only piecewise analytic separately in $\zeta > 0$ and $\zeta < 0$ with a nonanalyticity at $\zeta = 0$, originating from topological nature of this transition, in contrast to analytic expansions assumed in the LGW framework.

At nonzero temperatures $T \neq 0$, thermal fluctuations smear band-crossing points. The LGW form, $f[\zeta] - f[0] \simeq -\lambda\zeta + A\zeta^2 + B\zeta^4 + \mathcal{O}(\zeta^6)$ then recovers, leading to the Ising-type universality at $T > 0$.

Now we describe generic features of the phase diagram for OCT obtained from Eq. (5) in Fig.2(a) and for the honeycomb lattice in Fig.2(b). A semimetal (SM) is stabilized for a small interaction V_α ($\alpha = 1, 2$) (corresponding to $a > 0$ in Eq. (5)), at $\lambda = 0$ (along the white line in Fig.2(b)), while λ drives continuous quantum phase transitions to TI or CI at $\lambda \neq 0$. On the other hand, when

TABLE I. Singular part, order of transition, and critical exponents in doubly degenerate band-crossing point for several choices of band-dispersion exponent n and the spatial dimension d (for detailed derivation, see Supplemental Material S.2 [22]). First column shows f_s, singular parts in $f[\zeta]$. Second column shows order of transitions determined by following Ehrenfest's and Lifshitz's classifications. From 3rd to 5th columns, critical exponents around the QCP of TMT are shown. For $(n,d)=(1,3)$, exponents β and δ include logarithmic corrections denoted by ± 0, where $\zeta \simeq \pm\sqrt{|a|/b\ln 1/|a|}$ and $\zeta \simeq \mathrm{sign}(\lambda)\sqrt[3]{|\lambda|}\sqrt[3]{\frac{4b}{3}\ln 1/|\lambda|}$ for $|a|/t \ll 1$ and $|\lambda|/t \ll 1$. For $(n,d)=(2,2)$, "essential singular" means the instability by an infinitesimally small $V_\alpha/t \ll 1$. The pyrochlore belongs to (2,3), while it has some uniqueness partly because of the coexisting flat dispersions [22]. We note that singularities share similarities to several antiferromagnetic transitions in zero-gap semiconductors [23, 24].

		$f_s[\zeta]$	order of transition	$\zeta \propto \lvert a\rvert^\beta$	$\zeta \propto \lvert\lambda\rvert^{1/\delta}$	example
Dirac $(n=1)$	$d=2$	$\lvert\zeta\rvert^3$	3	$\beta=1$	$\delta=2$	honeycomb
	$d=3$	$\lvert\zeta\rvert^4\ln 1/\lvert\zeta\rvert$	4	$\beta=1/2-0$	$\delta=3+0$	
QBC $(n=2)$	$d=2$	$\lvert\zeta\rvert^2\ln\lvert\zeta\rvert$	(essential singular)	$\zeta \simeq \frac{\pm 1}{2vc_\alpha V_\alpha}\exp\left[-\frac{4vz_\alpha n_u}{c_\alpha^2 V_\alpha}\right]$	1	kagomé
	$d=3$	$\lvert\zeta\rvert^{5/2}$	2.5	$\beta=2$	$\delta=3/2$	pyrochlore

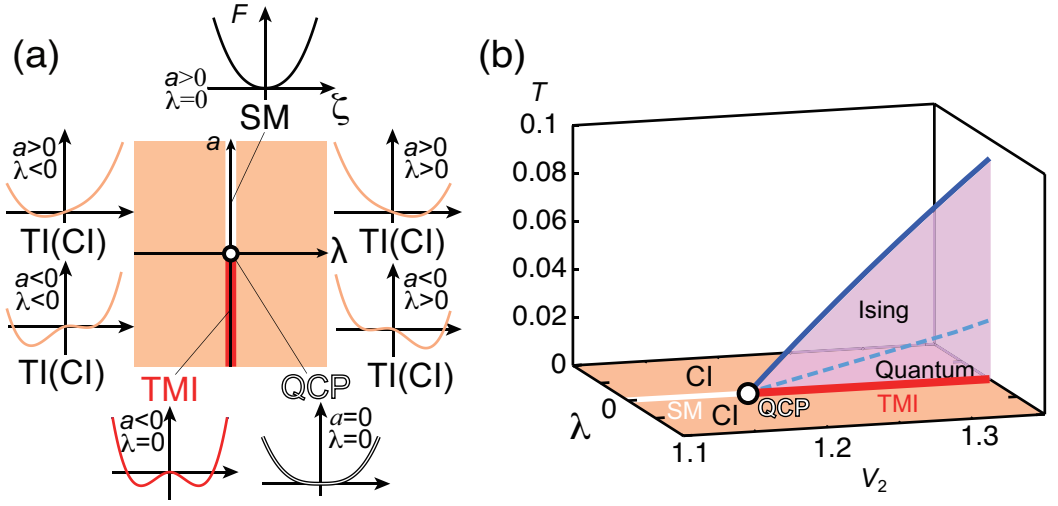

FIG. 2. (color online) (a) Schematic phase diagram in the plane of a proportional to interaction $V_c - V$ and conjugate field λ. Free energy structures in each phase representing topological insulators (TI), (Chern insulators (CI)), TMI and semimetal (SM) are also shown. (b) Phase diagram of CI induced by Coulomb-repulsion on honeycomb lattices in the space of temperature T, λ and interaction V_2 obtained by Hartree-Fock calculation. For the honeycomb case, the Chern-type TMI ($\zeta_c \neq 0, \zeta_s = 0$) and spin-orbit-type TMI ($\zeta_s \neq 0, \zeta_c = 0$) are degenerate on the mean-field level, while the Chern-type will win because of the discrete symmetry breaking, against the $SU(2)$ symmetry breaking of TMI, which is suppressed in 2D at $T > 0$. In the (pink) shaded area at $\lambda = 0$, the time-reversal symmetry is spontaneously broken and its border at $T \neq 0$ (the solid (blue) line) illustrates its critical line. This critical line follows the Ising universality (or in other words, maps to the gas-liquid transition). The dashed (blue) line shows a crossover between the quantum and Ising regions characterized by $\zeta \propto |a|$, and $\zeta \propto |a|^{1/2}$, respectively [25]. The white circle at $V = V_{2c} \simeq 1.18t$ and $\lambda = T = 0$ is the unconventional quantum critical point (QCP) of the TMT from which the white topological critical line (semimetal) at $T = 0$ and $\lambda = 0$ starts unlike the conventional QCP.

V_α exceeds the critical value $V_{\alpha c}$ (for $a < 0$), spontaneous orbital current (TMI phase) is stabilized for $\lambda = 0$ at $T = 0$, where the first-order transition separates $\lambda > 0$ and $\lambda < 0$. The first-order jump terminates at a line of Landau's critical temperature $T_c > 0$ This critical line (blue in Fig.2(b)) follows the Ising universality.

Sandwiched by Landau's (blue) line at $T_c > 0$ and the topological (white) line, a novel QCP (white circle) emerges. The critical exponents of the QCP are generically $\beta = n/(d-n)$, $\gamma = 1$ and $\delta = d/n$, indicating $\beta \geq 1/2$ and $\delta \leq 3$ (see Table I), completely opposite to the standard predictions of LGW symmetry-breaking transitions, which always satisfy $\beta \leq 1/2$ and $\delta \geq 3$. Here, β and δ are basic critical exponents to characterize how the order grows, as $\zeta \propto |a|^\beta$ at $\lambda = 0, a < 0$ and $\zeta \propto |\lambda|^{1/\delta}$ at $a = 0$, respectively. The present unusual universality is governed by the topology, similarly to the purely topological ones identified as the marginal quantum criticalities for Mott and Lifshitz transitions[5, 24, 25].

Strong correlation effects emerge as suppressions of simple orders with residual entropy and large quantum fluctuations at low temperatures. In the conventional systems with large Fermi surfaces, they emerge typically

as momentum and orbital differentiations as found in pseudogap and Fermi arc formation in the cuprate superconductors [26, 27]. In the zero-gap semiconductors, instead, large quantum fluctuations emerge quite differently as the unusual exponents such as large β and small δ, resulting in a slow and suppressed growth of the order, although the transition is strictly protected by the topological distinction at $T = 0$.

Now we consider an exceptional but interesting example of the pyrochlore lattice. Although the pyrochlore lattice has a unique feature [22], $f[\zeta]$ follows the same form as Eq. (5) with $f_s(\zeta_s) = |\zeta_s|^{5/2}$ and $0 < b_+ < b_-$. The obtained phase diagram in Fig.3 contains several distinct phases; SM, TMI (at $\lambda = 0, V > V_{1c}$), TI (at $\lambda > 0$) and TMI coexiting with charge order (TMI+CDW) (at $\lambda \leq 0, T = 0$). All the phases meet at the QCP (white circle), which follows a novel universality similar to the other lattices (see Table I). The extension of a critical line at T = 0 from the QCP (white lines in Figs.2 and 3) is common protected by the topological nature[5] and is fundamentally different from the LGW-type criticality even in itinerant electron systems [28–30] that does not have such a critical line and is simply described by $d + z$ dimensional classical LGW transitions, where z is the dynamical exponent. An important difference of Fig.3 from the *symmetric* case in Fig.2 is that the SM persists for $\lambda < 0$. In addition, a first-order transition surface (light green surface) (represented by $T = T_{1st}(\lambda, V_1)$) bends to $\lambda > 0$, which separates the *"topological semiconductor"* phase at $T > 0$ and $\lambda > 0$ into two: *Liquid-like* ($T < T_{1st}$) and *gas-like* ($T > T_{1st}$) semiconductors.

It is intriguing to associate the first-order transitions between gas- and liquid-like topological semiconductors (for $\lambda > 0$) as well as between SM and TMI+CDW (for $\lambda < 0$), to puzzling metal-semiconductor transitions in many pyrochlore compounds with bad metallic behavior as found in $Tl_2Ru_2O_7$ [18, 31] and $Ln_2Ir_2O_7$[32] for several lanthanoid elements Ln. Here, we have ignored the orbital degeneracy and orbital dependent anisotropy of transfers of the d bands, while in many cases basic structures at the band crossing are preserved even with this complexity. Indeed, triply degenerate bands at Γ point near the Fermi level shown in the local density approximation [31] supports the relevance of the present general theory. Whenever zero-gap semiconductors are found, our general scheme for (n, d) applies.

A nonzero spin-orbital current $|\zeta| \neq 0$ in the TMI breaks the rotational SU(2) invariance of the global spin quantization axis preserved in the original Hamiltonian. Therefore, the Nambu-Goldstone mode of this order is the spin rotation coupled to the orbital motion. We call this new collective excitation, *spin-orbiton*. The existence of the spin-orbiton is a way to distinguish TMIs from simple TIs induced by the spin-orbit couplings. Detecting whether such an excitation exists is an experimental challenge. In the SM phase, diverging spin-orbiton

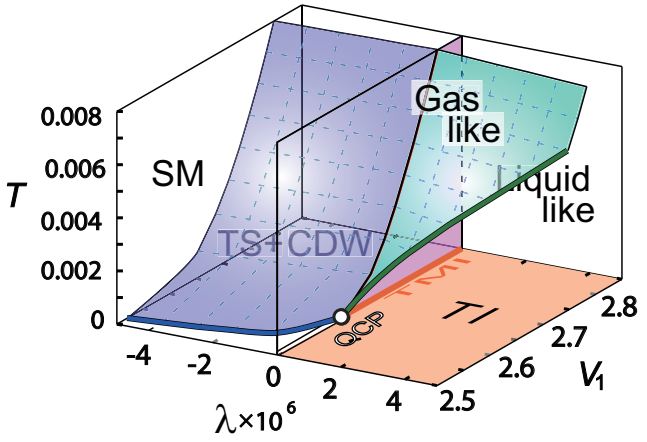

FIG. 3. (color) Phase diagram of pyrochlore lattice. When $\lambda = 0$, the system undergoes a transition from SM for small V_1 to TMI (dark orange line) at the QCP, $V_1 = V_{1c} \simeq 2.62$t at $T = 0$ (white circle). The QCP shows a new universality similar to Fig.2 beyond the LGW scheme. When $\lambda < 0$, SMs for small V_1 make a first-order transition (the light blue surface), to a topological semiconductor coexisting with charge order (TS+CDW). The TMI coexiting with charge order (TMI+CDW) at $\lambda \leq 0, T = 0$ crossovers to TS+CDW at finite temperatures. It terminates at a quantum critical line (dark blue). For $\lambda > 0$, a topological insulator with a gap is stabilized for all $V_1 \geq 0$ at $T = 0$. At $T > 0$, through a (light green) surface, ζ jumps.This surface separates a gas-like and liquid-like topological semiconductors (TS) and terminates on the Ising critical (bold green) line, which further terminates at the QCP. The QCP also terminates two quantum critical lines at $T = 0$, one along $\lambda = 0, V < V_{1c}$ (bold white line) and the other (the dark blue line) representing that between TS+CDW and SM. Here we note that, in the 3D lattices as the pyrochlore, the Chern-type TMI is not allowed and only the spin-current phase with $\zeta_s \neq 0$ is allowed [22].

fluctuations may couple to particle-hole excitations resulting in an overdamped mode, and alter the critical dynamics (dynamical exponent) [29]. This is an issue to be pursued.

Furthermore, spin-orbital currents that preserve the time reversal and lattice symmetries, are *invisible* in many standard experiments. TMI thus is a potential candidate of "hidden" orders behind mysterious insulating behaviors, as the orbital-current-induced pseudogap scenario discussed in cuprate physics [33, 34].

Summary. — Our findings present a solid foundation for unconventional critical phenomena of OCT, and serve a basis for utilization of the OCT such as switching between the topologically distinct phases. For more quantitative estimate of the critical exponents by considering fluctuations, for example, fermionic renormalization group[35] or a renormalization group method applicable to non-analytic free-energy expansions will be helpful and are left for future studies. Strong quantum fluctuations expected around the present OCT may offer a basis for unprecedented quantum phases mediated by the spin-

orbitons.

The authors thank financial support by Grant-in-Aid for Scientific Research (No. 22340090), from MEXT, Japan. Y.Y. thanks T. Misawa for fruitful discussions. A part of this research was supported by the Strategic Programs for Innovative Research (SPIRE), MEXT, and the Computational Materials Science Initiative (CMSI), Japan.

[1] L. D. Landau, E. M. Lifshitz, and E. M. Pitaevskii, *Statistical Physics* (Butterworth-Heinemann, New York, 1999).
[2] G.G. Wilson, Rev. Mod. Phys. **47**, 773 (1975).
[3] D. Belitz, T. R. Kirkpatrick, and T. Vojta, Rev. Mod. Phys. **77**, 579 (2005).
[4] T. Senthil, A. Vishwanath, L. Balents, S. Sachdev, and M. P. A. Fisher, Science **303**, 1490 (2004).
[5] M. Imada, T. Misawa, and Y. Yamaji, J. Phys: Cond. Matt. **22**, 164206 (2010) and references therein.
[6] A. H. Castro Neto, F. Guinea, N. M. R. Peres, K. S. Novoselov, and A. K. Geim, *Rev. Mod. Phys.* **81**, 109 (2009).
[7] L. Fu, C. L. Kane, and E. J. Mele, Phys. Rev. Lett. **98**, 106803 (2007) and references therein.
[8] J. E. Moore, and L. Balents, Phys. Rev. B **75**, 121306 (2007).
[9] R. Roy, Phys. Rev. B **79**, 195322 (2009).
[10] M. Z. Hasan, and C. L. Kane, Rev. Mod. Phys. **82**, 3045 (2010).
[11] T. Ando, T. Nakanishi, and R. Saito, J. Phys. Soc. Jpn. **67**, 2857 (1998).
[12] F. D. M. Haldane, Phys. Rev. Lett. **61**, 2015 (1988).
[13] K. S. Novoselov, *et al.* Nature **438**, 197 (2005).
[14] S. Ryu, C. Mudry, C.-Y. Hou, and C. Chamon, Phys. Rev. B **80**, 205319 (2009).
[15] J. Gonzalez, F. Guinea, and M. A. H. Vozmediano, Phys. Rev. B **63**, 134421 (2001).
[16] S. Raghu, X.-L. Qi, C. Honerkamp, and S.-C. Zhang, Phys. Rev. Lett. **100**, 156401 (2008).
[17] J. Wen, A. Rüegg, C.-C. J. Wang, and G. A. FietePhys. Rev. B, **82**, 075125 (2010).
[18] M. Kurita, Y. Yamaji, and M. Imada, J. Phys. Soc. Jpn. **80**, 044708 (2011).
[19] Y. Zhang, Y. Ran, and A. Vishwanath, Phys. Rev. B **79**, 245331 (2009).
[20] K. Sun, H. Yao, E. Fradkin, and S. A. Kivelson, Phys. Rev. Lett. **103**, 046811 (2009).
[21] H.-M. Guo, and M. Franz, Phys. Rev. Lett. **103**, 206805 (2009).
[22] See Supplemental Material at [URL] for details about orbital current mean field and free energy expansion.
[23] S. Sorella, and E. Tosatti, Europhys. Lett. **19**, 699 (1992).
[24] A. Bácsi, A. Virosztek, L. Borda, and B. Dóra, Phys. Rev. B **82**, 153406 (2010).
[25] T. Misawa, and M. Imada, Phys. Rev. B **75**, 115121 (2007).
[26] A. Damascelli, Z. Hussain and Z.X. Shen, Rev. Mod. Phys. **75**, 473 (2003)
[27] D.N. Basov, and T. Timusk, Rev. Mod. Phys. **77**, 721 (2005)
[28] T. Moriya, *Spin Fluctuations in Itinerant Electron Magnetism* (Springer-Verlag, Berlin, 1985).
[29] J. A. Hertz, Phys. Rev. B **14**, 1165 (1976).
[30] A. J. Millis, Phys. Rev. B **48**, 7183 (1993).
[31] F. Ishii, and T. Oguchi, J. Phys. Soc. Jpn. **69**, 526 (2000).
[32] K. Matsuhira, M. Wakeshima, R. Nakanishi, T. Yamada, A. Nakamura, W. Kawano, S. Takagi, and Y. Hinatsu, J. Phys. Soc. Jpn. **76**, 043706 (2007).
[33] S. Chakravarty, R. B. Laughlin, D. K. Morr, and C. Nayak, Phys. Rev. B **63**, 094503 (2001).
[34] C. M. Varma, Phys. Rev. B **73**, 155113 (2006).
[35] I. F. Herbut, V. Juricic, and O. Vafek. Phys. Rev. B **80**, 075432 (2009).

Supplemental Material

for "Breakdown of Landau-Ginzburg-Wilson scheme for phase transitions between orbital-current phases and zero-gap semiconductors "

by Moyuru Kurita, Youhei Yamaji, and Masatoshi Imada

In this Supplemental Material, we show theoretical methods used to derive our results in the main article. First, we show that the form of the orbital-current mean field is uniquely determined if we preserve the lattice and time-reversal symmetries. We next derive the free energy expansions for general degenerate band crossings and apply them to some specific examples, a honeycomb, kagomé and pyrochlore lattices. As is introduced in the main article, we start from an extended Hubbard model on these lattices,

$$\hat{H} = -t \sum_{\langle i,j\rangle\sigma} \hat{c}^\dagger_{i\sigma}\hat{c}_{j\sigma} + U\sum_i \hat{n}_{i\uparrow}\hat{n}_{i\downarrow} + \sum_{i,j}\frac{V_{ij}}{2}\hat{n}_i\hat{n}_j. \tag{S.1}$$

S.1 ORBITAL-CURRENT MEAN FIELD

Here, we show that the spin-orbit interaction as well as the orbital-current mean-field has a unique form if we preserve the lattice and time reversal symmetries. Let us first consider some symmetry operations satisfied by honeycomb, kagomé, and pyrochlore lattices. When we pick up a bond between i-th ($\vec{r}_i$) and j-th sites ($\vec{r}_j$) of a lattice, the system is invariant under 3 important symmetric operations related to the bond: (1) The time reversal operation Θ, (2) a reflection with respect to a plane perpendicular to the bond and containing the center of the bond, which is denoted by $R^\perp_{(i,j)}$ (3) a 180°-rotation around the axis perpendicular to the bond and crossing at the center of the bond each other, which is denoted as $R^{180^\circ}_{(i,j)}$. For all the lattices considered, the axis for $R^{180^\circ}_{(i,j)}$ that keeps the lattice invariant is along the vector $\vec{b}_{ij}$ pointing to the center of the bond (i,j) from the gravity center $\vec{o}_{ij}$ of the unit cell containing i and j (see Fig.S1). This is defined as $\vec{b}_{ij} = (\vec{r}_i + \vec{r}_j)/2 - \vec{o}_{ij}$. For the honeycomb, kagomé and pyrochlore lattices, $\vec{o}_{ij}$ is the gravity center of the hexagon, triangle and tetrahedron, respectively, as illustrated in Fig.S1(a)-(c).

Next we introduce a current flowing through the bond (i,j) along $\vec{d}_{ij} = \vec{r}_i - \vec{r}_j$, described by the hermitian charge/spin current operator $\hat{J}^{(a)}_{(i,j)} (= [\hat{J}^{(a)}_{(i,j)}]^\dagger)$ defined by

$$\hat{J}^{(a)}_{(i,j)} = (-i)\sum_{\alpha,\beta=\uparrow,\downarrow}\left[\hat{c}^\dagger_{i\alpha}\hat{\sigma}^{(a)}_{\alpha\beta}\hat{c}_{j\beta} - \hat{c}^\dagger_{j\alpha}\hat{\sigma}^{(a)}_{\alpha\beta}\hat{c}_{i\beta}\right]. \tag{S.2}$$

Here, a 2×2 matrix $\hat{\sigma}^a$ represents, for $a = 0$, a 2D identity matrix describing the charge current or, for $a = x, y, z$, Pauli matrices describing the spin currents.

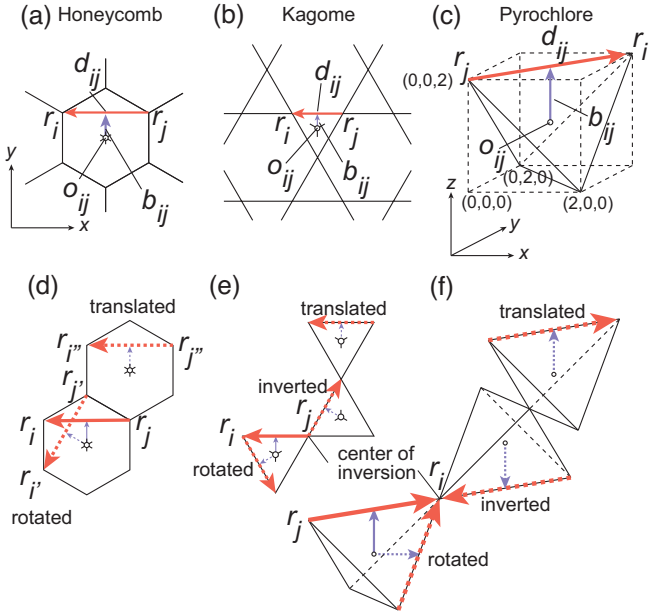

Fig. S 1. (a)-(c) Examples for vectors $\vec{r}_i$, $\vec{r}_j$, $\vec{o}_{ij}$, $\vec{b}_{ij}$, and $\vec{d}_{ij}$ for the honeycomb, kagomé and pyrochlore lattice. (d)-(f) Examples of symmetric operations applied to a bond (i,j).

Let us examine symmetric properties of $\hat{J}^{(a)}_{(i,j)}$. As charge currents break the time-reversal symmetry while spin currents preserve it, $\hat{J}^{(0)}_{(i,j)}$ and $\hat{J}^{(x,y,z)}_{(i,j)}$ are time-reversal odd and even, respectively.

Similarly, the reflection $R^\perp_{(i,j)}$ and the rotation $R^{180^\circ}_{(i,j)}$ transform $\hat{J}^{(0)}_{(i,j)}$ into $R^\perp_{(i,j)}[\hat{J}^{(0)}_{(i,j)}] = R^{180^\circ}_{(i,j)}[\hat{J}^{(0)}_{(i,j)}] = -\hat{J}^{(0)}_{(i,j)}$. Therefore we note that, if the lattice symmetry satisfies these reflection and rotation as symmetric operations, the charge-current mean field breaks the reflection/rotation symmetry in addition to the time-reversal symmetry. When the charge currents form a loop, after setting currents on every bond as we will discuss below, these currents break the so-called chiral symmetry.

On the other hand, spin current operators $\hat{J}^{(x,y,z)}_{(i,j)}$ are transformed in complicated ways: The reflection $R^\perp_{(i,j)}$ makes a spin rotate 180° around $\vec{d}_{ij}$, while $R^{180^\circ}_{(i,j)}$ makes the spin rotate 180° around $\vec{b}_{ij}$. In addition, the both operations exchange the sites i and j. For example, if we take $\vec{d}_{ij} = (-|\vec{d}_{ij}|, 0, 0)$ and $\vec{b}_{ij} = (0, |\vec{b}_{ij}|, 0)$, the reflection $R^\perp_{(i,j)}$ transforms a vector $(\hat{J}^{(x)}_{(i,j)}, \hat{J}^{(y)}_{(i,j)}, \hat{J}^{(z)}_{(i,j)})$ into $(-\hat{J}^{(x)}_{(i,j)}, \hat{J}^{(y)}_{(i,j)}, \hat{J}^{(z)}_{(i,j)})$, while the rotation $R^{180^\circ}_{(i,j)}$ transforms it into $(\hat{J}^{(x)}_{(i,j)}, -\hat{J}^{(y)}_{(i,j)}, \hat{J}^{(z)}_{(i,j)})$. Thus, if a spin current preserves the two symmetries, the spin alignment vector $\vec{n}_{(i,j)}$ of the current from j-th to i-th sites, has to be along the z-axis. More generally, when the above three symmetries are preserved, the unit vector $\vec{n}_{(i,j)}$ has to be perpendicular to both of $\vec{d}_{ij}$ and $\vec{b}_{ij}$ and uniquely has the

form $\vec{n}_{(i,j)} = \pm\vec{b}_{ij} \times \vec{d}_{ij}/|\vec{b}_{ij} \times \vec{d}_{ij}|$.

Now, the spin current operator is expressed by

$$\hat{J}^{(s)}_{(i,j)}(\vec{n}_{(i,j)}) = n^{(x)}_{(i,j)}\hat{J}^{(x)}_{(i,j)} + n^{(y)}_{(i,j)}\hat{J}^{(y)}_{(i,j)} + n^{(z)}_{(i,j)}\hat{J}^{(z)}_{(i,j)}$$
$$= (-i)\sum_{\alpha,\beta}\left[\hat{c}^{\dagger}_{i\alpha}\{\vec{n}_{(i,j)}\cdot\vec{\sigma}\}_{\alpha\beta}\hat{c}_{j\beta} - \hat{c}^{\dagger}_{j\alpha}\{\vec{n}_{(i,j)}\cdot\vec{\sigma}\}_{\alpha\beta}\hat{c}_{i\beta}\right]. \tag{S.3}$$

We also note that for the honeycomb lattice, the bond (i,j) has to be between the 2nd neighbor sites, because the nearest-neighbor and the 3rd-neighbor bonds have an additional 180°-rotation symmetry with the axis crossing the honeycomb plane perpendicularly at the center of the bond. This symmetry prohibits the currents even in the $\vec{b}_{ij} \times \vec{d}_{ij}$ direction. In a similar way, for the kagomé and pyrochlore lattices, $\vec{d}_{ij} \neq \vec{0}$ (i,j) has to be between the nearest-neighbor sites. (See Fig.1(a)-(c).)

After choosing the direction and spin alignment of the flow, we apply a symmetry operation, which belongs to the point group of the underlying lattice, to the bond (i,j). For example, in the honeycomb lattice, every 2nd-neighbor bond, where orbital currents flow, is involved in a hexagon. A 6-fold rotation (C_6 rotation), around the center of such a hexagon, $\vec{o}_{ij}$, is one of the examples of symmetric operations. If we apply the C_6 rotation, we obtain the bond (i',j') shown in Fig.1(d). After successive applications of C_6 rotations around $\vec{o}_{ij}$, we can determine the direction and spin alignment of the flow of 5 more bonds involved in the hexagon. Under these operations, $\vec{o}_{ij}$ is invariant, and $\vec{b}_{ij}$ and $\vec{d}_{ij}$ are transformed into, for example, $\vec{b}_{i'j'}$ and $\vec{d}_{i'j'}$, respectively. If we further use the translational invariance of the honeycomb lattice, we can determine the direction and spin alignment of the flow for all of the 2nd neighbor bonds on the lattice. For example, we obtain the bond $(i",j")$ by translating the bond (i,j) shown in Fig.1(d). Simultaneously, vectors $\vec{b}_{ij}$ and $\vec{d}_{ij}$ are transformed into $\vec{b}_{i"j"}$ and $\vec{d}_{i"j"}$ as well. When the unit cells share their corner, for a kagomé and pyrochlore lattice, the inversion operations shown in Fig.1(e) and (f) can be used.

Then an explicit expression for orbital-current mean fields with a magnitude ζ, together with a hopping renormalization g due to a usual Fock term is obtained from Eq. (S.2) for the spin-orbital-current mean field

$$\left\langle \hat{c}^{\dagger}_{j\beta}\hat{c}_{i\alpha}\right\rangle = g\delta_{\alpha\beta} - i\zeta\frac{\vec{b}_{ij}\times\vec{d}_{ij}}{|\vec{b}_{ij}\times\vec{d}_{ij}|}\cdot\vec{\tilde{\sigma}}_{\alpha\beta}, \tag{S.4}$$

which creates the topological insulators, or a charge-orbital-current mean field,

$$\left\langle \hat{c}^{\dagger}_{j\beta}\hat{c}_{i\alpha}\right\rangle = \left(g - i\zeta\left[\frac{\vec{b}_{ij}\times\vec{d}_{ij}}{|\vec{b}_{ij}\times\vec{d}_{ij}|}\right]_z\right)\delta_{\alpha\beta}, \tag{S.5}$$

which induces the Chern insulators (absent in 3D lattices). These mean fields are generated through a decoupling of the two-body interaction term,

$$\hat{n}_{i\alpha}\hat{n}_{i\beta} \to \langle\hat{n}_{i\alpha}\rangle\hat{n}_{j\beta} + \hat{n}_{i\alpha}\langle\hat{n}_{j\beta}\rangle - \langle\hat{n}_{i\alpha}\rangle\langle\hat{n}_{j\beta}\rangle$$
$$-\left\langle\hat{c}^{\dagger}_{i\alpha}\hat{c}_{j\beta}\right\rangle\hat{c}^{\dagger}_{j\beta}\hat{c}_{i\alpha} - \hat{c}^{\dagger}_{i\alpha}\hat{c}_{j\beta}\left\langle\hat{c}^{\dagger}_{j\beta}\hat{c}_{i\alpha}\right\rangle + \left|\left\langle\hat{c}^{\dagger}_{i\alpha}\hat{c}_{j\beta}\right\rangle\right|^2. \tag{S.6}$$

Here we note that the orbital-currents instabilities compete with charge and/or spin density wave instabilities in real lattice structures. Many studies were carried out to search the conditions that an orbital-current phase becomes a stable mean-field ground state as discussed by S. Raghu, X.-L. Qi, C. Honerkamp, and S.-C. Zhang, Phys. Rev. Lett. **100**, 156401 (2008), J. Wen, A. Rüegg, C.-C. J. Wang and G. A. Phys. Rev. B **82**, 075125 (2010), and M. Kurita, Y. Yamaji, and M. Imada, J. Phys. Soc. Jpn. **80**, 044708 (2011) (Refs.16-18 of main article). For instance, the spin-orbital currents are stabilized for reasonably realistic values, $4.5 \lesssim U/t \lesssim 6$ and $2.5 \lesssim V_1/t \lesssim 3$ for a pyrochlore lattice with one electron per site.

S.2 FREE ENERGY EXPANSION

Based on orbital-current mean fields given in Eqs. (S.4) and (S.5), the mean-field hamiltonian for specific lattices is derived, with an appropriate choice of parameters, for example, (U, V_1, V_2). First, we derive a general and simple analytic formulae of free-energy expansions for doubly-degenerate band crossings, by focusing on low-energy band dispersion around band-crossing points. It is applied to the case of the honeycomb and kagomé lattices. Second, we give a free energy expansion for a triply-degenerate band crossing and applies to the pyrochlore lattice. We also refer to a peculiar inversion of valence and conduction bands in a pyrochlore lattice occurring by the sign change of the spin orbital current, ζ. Here, we note that the transition discussed in this article is different from that between the topological and band insulators discussed by S. Murakami, New J. Phys. **12**, 065008 (2007).

Doubly degenerate band crossings

When magnitude of an orbital current ζ between α-th neighbor sites becomes finite, two bands split in the momentum space, $\epsilon_{\pm}[\zeta](\vec{p})$, with a gap scaled by $|\zeta|$. Then we obtain a mean-field free energy per unit cell as,

$$f[\zeta] = \frac{F[\zeta]}{N_u} = -\frac{2k_{\rm B}T}{N_u}\sum_{\vec{p}}\left\{\ln\left[1 + e^{-(\epsilon_+[\zeta](\vec{p})-\mu)/k_{\rm B}T}\right]\right.$$
$$\left. + \ln\left[1 + e^{-(\epsilon_-[\zeta](\vec{p})-\mu)/k_{\rm B}T}\right]\right\} + z_\alpha n_{\rm u} V_\alpha \zeta^2, \tag{S.7}$$

where N_u is the number of unit cells, z_α is the coordination number of the α-th neighbor site, $n_{\rm u}$ is the number of sites in an unit cell, and V_α is the Coulomb repulsion between α-th neighbor sites. The chemical potential μ is chosen to keep electron density or filling listed in Table SI to keep the valence band ϵ_- fully-filled at $T=0$.

Here we focus on a small energy window around a band crossing point $\vec{p}_{\rm BC}$, and introduce a cutoff Λ, which does not change any essential physics. If we choose a proper Λ for each lattice, full numerical results for the original microscopic hamiltonian are quantitatively reproduced. Then we can expand the band dispersion $\epsilon_\pm$ with respect to the momentum measured from the band crossing point, $\vec{k}$ as

$$\epsilon_\pm[\zeta](\vec{p}_{\rm BC}+\vec{k}) \simeq \epsilon(\vec{k}) \pm \sqrt{m^2 + v_\pm^2 |\vec{k}|^{2n}}, \quad \text{(S.8)}$$

where a "mass" m is given as $m = c_\alpha V_\alpha \zeta$ with a coefficient c_α. The dispersion $\epsilon(\vec{k})$, coefficient c_α, and "velocities" $v_\pm$ depending on the lattices are listed in Table SI.

At $T=0$, the free energy has a simple analytic form,

$$\frac{F[\zeta]-F[0]}{N_u} \simeq \frac{2n_{\rm BC}\Omega_d}{V_{\rm BZ}} Q + z_\alpha n_{\rm u} V_\alpha \zeta^2, \quad \text{(S.9)}$$

$$Q = \int_0^\Lambda k^{d-1} dk \left[-\sqrt{m^2 + v_-^2 k^{2n}} + v_- k^n \right] \quad \text{(S.10)}$$

where $k = |\vec{k}|$, $n_{\rm BC}$ is the number of band-crossing points, $V_{\rm BZ}$ is the volume of the Brillouin zone, and $\Omega_d = 2\pi$ (4π) for $d=2$ $(d=3)$.

Singular part of the free energy arises from

$$Q = v_- |m|^{\frac{d}{n}+1} \int_0^{\Lambda/|m|^{\frac{1}{n}}} q^{n+d-1} dq \left[1 - \sqrt{1 + \frac{1}{v_-^2 q^{2n}}} \right], \quad \text{(S.11)}$$

where we rescale the integration variable as $q = k/|m|^{1/n}$ to absorb the singular m dependence out of the integrand. Here we note that the integral in the right hand side of Eq. (S.11) causes ultra-violet divergences in the limit $|m| \to 0+$, for $n \le d$, which is compensated by the prefactor $|m|^{d/n+1}$ but leaves the singularity. In fact, by expanding the integrand in power of $1/q^{2n}$, Q turns out to have series of singular terms $\propto |m|^{2\ell+1-d/n}$ with any integer $\ell \ge 0$, which yields a singular expansion in terms of ζ.

For example, for the honeycomb lattice with $(n,d) = (1,2)$, namely, for $d/n+1 = 3$, we obtain a non-Ginzburg-Landau-Wilson-type free energy expansion as

$$\frac{F[\zeta]-F[0]}{N_u} \simeq a\zeta^2 + b|\zeta|^3 + \text{(higher order)}, \quad \text{(S.12)}$$

where the coefficients a and b are given in Table SI.

For $d = (2\ell+1)n$, the integral Eq. (S.11) yields a logarithmic correction proportional to $\ln|\zeta|$. Indeed, for $n=d$, we obtain the free energy expansion as

$$\frac{F[\zeta]-F[0]}{N_u} \simeq b\zeta^2 \ln|\zeta| + a\zeta^2 + \text{(higher order)}, \quad \text{(S.13)}$$

where the coefficients a and b are given in Table SI for the kagomé lattice with $(n,d) = (2,2)$.

The band crossing satisfying $d = 3n$ or $(n,d) = (1,3)$ is not known in the real lattice to our knowledge. We can, however, predict a general form of the expansion as

$$\frac{F[\zeta]-F[0]}{N_u} \simeq \frac{2n_{\rm BZ}\Omega_d}{V_{\rm BZ}} \left[\frac{z_\alpha n_{\rm u}}{c_\alpha^2 V_\alpha} - \frac{3}{4dv_-} \Lambda^{2d/3} \right] c_\alpha^2 V_\alpha^2 \zeta^2 + \frac{2n_{\rm BZ}\Omega_d}{V_{\rm BZ}} \frac{c_\alpha^4 V_\alpha^4}{4dv_-^3} \zeta^4 \ln\frac{1}{|\zeta|} + \text{(higher order)}. \quad \text{(S.14)}$$

Triply degenerate band crossings: pyrochlores

Now we give a free-energy expansion for the pyrochlore lattice, as an example of the case $(n,d) = (2,3)$.

The mean-field hamiltonian for topological Mott states is given as

$$\hat{H}_{\rm mf} = \sum_{\vec{k}} \vec{\hat{\Phi}}_{\vec{k}}^\dagger [\overleftrightarrow{h}_0(\vec{k}) + V_1 \overleftrightarrow{j}_\zeta(\vec{k})] \vec{\hat{\Phi}}_{\vec{k}}, \quad \text{(S.15)}$$

where the 8×8 Bloch hamiltonian $\overleftrightarrow{h}_0(\vec{k})$ for a non-interacting electrons on a pyrochlore lattice is given by

$$\overleftrightarrow{h}_0(\vec{k}) = -2t' \mathbf{1}_2 \otimes \begin{bmatrix} 0 & \cos(k_x-k_y) & \cos(k_y-k_z) & \cos(k_z+k_x) \\ \cos(k_x-k_y) & 0 & \cos(k_z-k_x) & \cos(k_y+k_z) \\ \cos(k_y-k_z) & \cos(k_z-k_x) & 0 & \cos(k_x+k_y) \\ \cos(k_z+k_x) & \cos(k_y+k_z) & \cos(k_x+k_y) & 0 \end{bmatrix}, \quad \text{(S.16)}$$

with a spin-independent renormalized hopping matrix $t' = t + V_1 \left\langle \hat{c}_{i\sigma}^\dagger \hat{c}_{j\sigma} \right\rangle$ and a 2×2 unit matrix $\mathbf{1}_2$ acting on the

Table S I. Summary of band dispersions, parameters depending on lattice structures, and coefficients for the free energy expansions. The cutoff Λ for the kagomé lattice ($(n,d)=(2,2)$) is numerically not accurately determined yet, because of a numerical difficulty in the essential singular behavior.

	honeycomb $(n,d)=(1,2)$	kagomé $(n,d)=(2,2)$	pyrochlore $(n,d)=(2,3)$
filling	one electron per site	4/3 electrons per site	one electron per site
$\epsilon(\vec{k})$	0	$2t'-t'k^2/2$	-
c_α	$3\sqrt{3}$	$2\sqrt{3}$	-
v_-	$\sqrt{3}t$	$t'/2$	-
α	2	1	1
z_α	6	4	6
$n_{\rm BC}$	2	1	1
n_u	2	3	4
$V_{\rm BZ}$	$\frac{2\pi^2}{\sqrt{3}}$	$\frac{2\pi^2}{\sqrt{3}}$	$\frac{\pi^3}{4}$
a	$12V_2-\frac{54\Lambda V_2^2}{\pi t}$	$12V_1-\frac{6\sqrt{3}V_1^2}{\pi t'}\left[1+2\ln\left(\frac{t'\Lambda^2}{2\sqrt{3}V_1}\right)\right]$	$24V_1-\frac{256V_1^2\Lambda}{\pi^2 t'}$
b	$b_\pm=\frac{108V_2^3}{\pi t^2}$	$b_\pm=-\frac{12\sqrt{3}V_1^2}{\pi t'}$	$b_+=9.37t'\left(\frac{V_1}{t'}\right)^{\frac{5}{2}}\quad b_-=55.4t'\left(\frac{V_1}{t'}\right)^{\frac{5}{2}}$
Λ	0.590	$*$	0.507

spin degrees of freedom. The spin orbital current $\overleftrightarrow{j}_\zeta(\vec{k})$ is given by a 8×8-matrix,

$$\overleftrightarrow{j}_\zeta(\vec{k})=\sqrt{2}i\zeta\begin{bmatrix}0 & u_{xy} & -u_{yz} & v_{zx}\\ -u_{xy} & 0 & u_{zx} & v_{yz}\\ u_{yz} & -u_{zx} & 0 & v_{xy}\\ -v_{zx} & -v_{yz} & -v_{xy} & 0\end{bmatrix}, \tag{S.17}$$

with

$$u_{ij}=(\hat{\sigma}_i+\hat{\sigma}_j)\cos(k_i-k_j), \tag{S.18}$$

$$v_{ij}=(\hat{\sigma}_i-\hat{\sigma}_j)\cos(k_i+k_j). \tag{S.19}$$

Here $\vec{\hat{\Phi}}^\dagger_{\vec{k}}=(\hat{c}^\dagger_{1\vec{k}\uparrow},\hat{c}^\dagger_{1\vec{k}\downarrow},\hat{c}^\dagger_{2\vec{k}\uparrow},\hat{c}^\dagger_{2\vec{k}\downarrow},\hat{c}^\dagger_{3\vec{k}\uparrow},\hat{c}^\dagger_{3\vec{k}\downarrow},\hat{c}^\dagger_{4\vec{k}\uparrow},\hat{c}^\dagger_{4\vec{k}\downarrow})$ represents a vector notation of the creation operators of the Bloch states, with the suffix 1 to 4 in the creation operators representing the 4 sites of the unit cell.

By diagonalizing the mean-field hamiltonian, we obtain 4 bands. Out of the 4 bands, we focus on 3 bands touching each other at the Γ point. In contrast to simple conduction- and valence-band dispersions already discussed, here, we need to handle 3 bands for $\zeta=0$,

$$\epsilon=2t',2t',2t'-2t'k^2+\mathcal{O}(k^4). \tag{S.20}$$

By considering the spin degenracy, we have 6 bands touching at the band crossing point.

In the presence of non-zero spin orbital currents $\zeta\neq 0$, we obtain 3 split bands,

$$\epsilon=2t'+2\sqrt{2}V_1\zeta,2t'-\sqrt{2}V_1\zeta-t'k^2 \pm\sqrt{(\sqrt{2}V_1\zeta-t'k^2)^2+16V_1^2\zeta^2}, \tag{S.21}$$

where the hopping matrix t is renormalized as $t'=t+V_1\left\langle\hat{c}^\dagger_{i\sigma}\hat{c}_{j\sigma}\right\rangle$. Each dispersion is doubly degenerate. At the Γ point of the Brillouin zone, $k=0$, in terms of the group theory, 6 degenerate bands in the $T\otimes SU(2)$-manifold split into a doublet ($E_{5/2}$) and quartet ($G_{3/2}$), due to spin orbital currents.

As it has been already mentioned by H.-M. Guo, and M. Franz, Phys. Rev. Lett. **103**, 206805 (2009) (Ref.21 of main article), for non-interacting electrons with spin-orbit couplings on pyrochlores, the sign of ζ is crucial whether the system becomes topological insulators or not. We note that, for the honeycomb and kagomé lattices, topological Mott states appear for both positive and negative ζ. However, for the pyrochlore lattice, the sign of ζ reverses the level of the doublet $E_{5/2}$ and quartet $G_{3/2}$. Only if the doublet $E_{5/2}$ becomes occupied, the system becomes a topological Mott insulator.

Then the free energy at $T=0$ is given by

$$\frac{F[\zeta]-F[0]}{N_u}\simeq+\frac{32}{\pi^2}\int_0^\Lambda dkk^2\left(t'k^2-\sqrt{2}V_1\zeta-\sqrt{(t'k^2-\sqrt{2}V_1\zeta)^2+16V_1^2\zeta^2}\right)+24V_1\zeta^2. \tag{S.22}$$

From this form of the free energy, we have

$$\frac{\partial^2 F}{N_u \partial \zeta^2}(\zeta = 0) = -\frac{512 V_1^2 \Lambda}{\pi^2 t'} + 48 V_1 \tag{S.23}$$

and

$$\frac{\partial^3 F}{N_u \partial \zeta^3} = \frac{1536 t'}{\pi^2 \sqrt{|\zeta|}} \left(\frac{V_1}{t'}\right)^{\frac{5}{2}} \int_0^{\sqrt{\frac{t'}{V_1|\zeta|}}\Lambda} dx \frac{x^6 (18 - \mathrm{sgn}(\zeta)\sqrt{2}x^2)}{(18 - \mathrm{sgn}(\zeta) 2\sqrt{2}x^2 + x^4)^{\frac{5}{2}}} \tag{S.24}$$

from which the energy expansion is given by

$$\frac{F(\zeta)}{N_u} = \frac{F(0)}{N_u} + a\zeta^2 + b_\pm |\zeta|^{\frac{5}{2}} + \mathcal{O}(\zeta^4), \tag{S.25}$$

where a and $b_\pm$ are summarized in Table SI.